Electronic Supplementary Information

Relaxor Ferroelectric Polymer with Ultrahigh Dielectric Constant Largely Promotes the Dissociation of Lithium Salts to Achieve High Ionic Conductivity

Yan-Fei Huang[a,b], Tian Gu[a,c], Guanchun Rui[d], Peiran Shi[a,c], Wenbo Fu[e], Chen Lai[f], Xiaotong Liu[a,c], Jianping Zeng[b], Benhao Kang[b], Zhichao Yan[b], Florian J. Stadler[b], Lei Zhu[c], Feiyu Kang[a,c], Yan-Bing He[a,]*

[a] Shenzhen Geim Graphene Center, Institute of Materials Research, Tsinghua Shenzhen International Graduate School, Tsinghua University, Shenzhen, 518055, P. R. China.

[b] Shenzhen Key Laboratory of Polymer Science and Technology, Guangdong Research Center for Interfacial Engineering of Functional Materials, College of Materials Science and Engineering, Shenzhen University, Shenzhen 518055, P. R. China

[c] Laboratory of Advanced Materials, Department of Materials Science and Engineering, Tsinghua University, Beijing, 100084, P. R. China.

[d] Department of Macromolecular Science and Engineering, Case Western Reserve University, Cleveland, Ohio 44106-7202, United States

[e] Jingtai Technology Co., Ltd., Shenzhen, 518055, P. R. China.

[f] Key Lab of Advanced Functional Materials, Ministry of Education, Faculty of Materials and Manufacturing, Beijing University of Technology, Beijing, 100124, P. R. China.

Corresponding author. E-mail: he.yanbing@sz.tsinghua.edu.cn (Y.-B He)

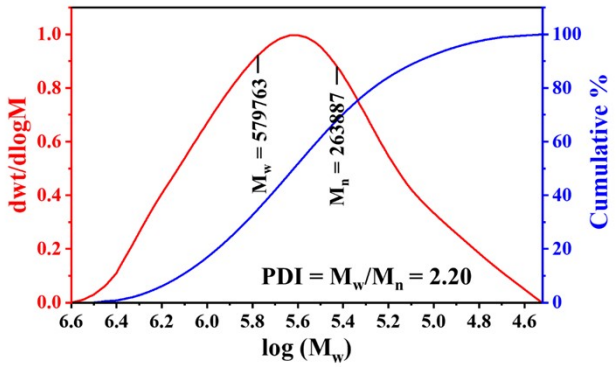

Fig. S1. GPC molecular weight distribution of P(VDF-TrFE-CTFE). DMF was used as the solvent with a flow rate of 1.0 mL/min.

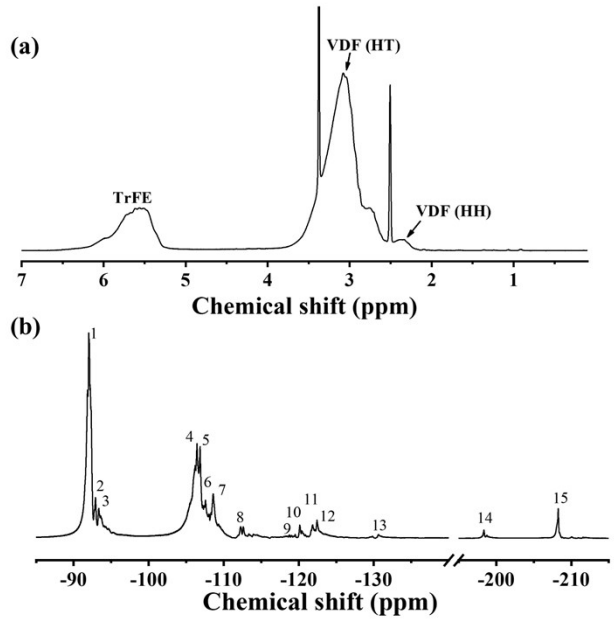

Fig. S2. (a) ^{1}H and (b) ^{19}F NMR spectra (DMSO-d_6) for the P(VDF-TrFE-CTFE) 65.4/26.2/8.4 terpolymer. ^{19}F NMR peak assignments for the terpolymer are listed in Table S1.

From the ^{1}H NMR spectroscopy (Fig. S2a), the peaks at about 5.6, 3.1, and 2.4 ppm are assigned to TrFE, -$CF_2CH_2CF_2CH_2CF_2$- sequence [VDF (HT)], and -$CH_2CF_2CF_2CH_2$- sequence [VDF (HH)], respectively.[S1] The peaks at 2.5 and 3.3 ppm are assigned to DMSO-d_6 and water, respectively. From the ^{19}F NMR results (Fig. S2b and Table S1), the molar compositions were determined. It was found that the main structure of the terpolymer includes VDF-VDF head-to-tail sequence (-$CF_2CH_2CF_2CH_2CF_2$-), CTFE-CTFE head-to-tail sequence

(-$CF_2CClFCF_2CClFCF_2$-), and VDF-CTFE tail-to-tail sequence (-$CF_2CH_2CF_2CF_2CClF$-). ^{19}F NMR peak assignments for the P(VDF-TrFE-CTFE) are listed in Table S1.

Table S1. ^{19}F NMR Peak Assignments for P(VDF-TrFE-CTFE) 65.4/26.2/8.4 terpolymer.

Peak No.	Sequence	Designation*	Chemical Shift (ppm)	Percentage (%)
1	-$CF_2CH_2CF_2CH_2CF_2$-	VDF-VDF/H-T	-92.02	37.88
2	-$CF_2CH_2CF_2CH_2CF_2$-	VDF-VDF/H-T	-92.90	3.40
3	-$CHFCH_2CF_2CH_2CF_2$- -$ClFCH_2CF_2CH_2CF_2$-	TrFE-VDF/T-T CTFE-VDF/T-T	-93.34 ~ -93.66	4.17
4	-$CF_2CClFCF_2CClFCF_2$-	CTFE-CTFE/H-T	-106.38	13.64
5	-$CF_2CHFCF_2CH_2CF_2$-	TrFE-VDF/H-T	-106.84	7.95
6	-$CH_2CH_2CF_2CHFCF_2$-	VDF-TrFE/H-T	-107.56	5.68
7	-$CF_2CH_2CF_2CF_2CClF$-	VDF-CTFE/T-T	-108.58	9.09
8	-$CF_2CH_2CF_2CF_2CHF$-	VDF-TrFE/T-T	-112 ~ -112.84	1.89
9	-$CH_2CF_2CF_2CClFCH_2$-	VDF-CTFE/T-T	-118.74 ~ -119.53	0.76
10	-$CHFCF_2CF_2CFClCH_2$-	TrFE-CTFE-VDF/T-T-T	-120.26	1.52
11	-$CF_2CHFCF_2CHF_2CF_2$-	TrFE-TrFE/H-T	-121.83	1.52
12	-$CHFCHFCF_2CF_2CHF$-	TrFE-TrFE/T-T	-122.43	2.73
13	-$CF_2CFClCF_2CHFCH_2$-	CTFE-TrFE-VDF/H-T-T	-130.73	0.76
14	-$CF_2CF_2CHFCH_2CF_2$-	TrFE-VDF/T-T	-198.35	0.76
15	-$CH_2CF_2CHFCF_2CH_2$-	VDF-TrFE/H-T	-208.26	2.27

Note: Peak assignments are referenced from: Lu, Y. Y.; Claude, J.; Zhang, Q. M.; Wang, Q. *Macromolecules* **2006,** *39*, 6962-6968.; Yang L.; Tyburski B. A.; Dos Santos F. D., et al. *Macromolecules* **2014**, *47*, 8119-8125.

First, the P(VDF-TrFE-CTFE) SPEs films were prepared at 50, 55, and 60 ^oC for 25 h, respectively. The ionic conductivity of the P(VDF-TrFE-CTFE) SPEs prepared at 50, 55, and 60 ^oC was measured as 4.9×10^{-4}, 3.1×10^{-4}, and 2.6×10^{-4} S cm^{-1}, respectively (Fig. S3a). TGA was employed to detect the amount of residual DMF in these three samples, as shown in

Fig. S3b. The minor weight loss before 55 °C (region I) is due to the trapped moisture. The weight loss observed at 55-200 °C (region II) derives from the evaporation of residual DMF.[S2] The residue of DMF is estimated about 11.2%, 9.9 wt% and 7.7 wt% in P(VDF-TrFE-CTFE) SPEs prepared at 50, 55, and 60 °C, respectively. The increase of DMF content in P(VDF-TrFE-CTFE) SPEs can enhance the ionic conductivities but also leads to a high side reaction of P(VDF-TrFE-CTFE) SPEs with both anode and cathode. Therefore, 55 °C is employed to prepare the P(VDF-TrFE-CTFE) SPEs in this work.

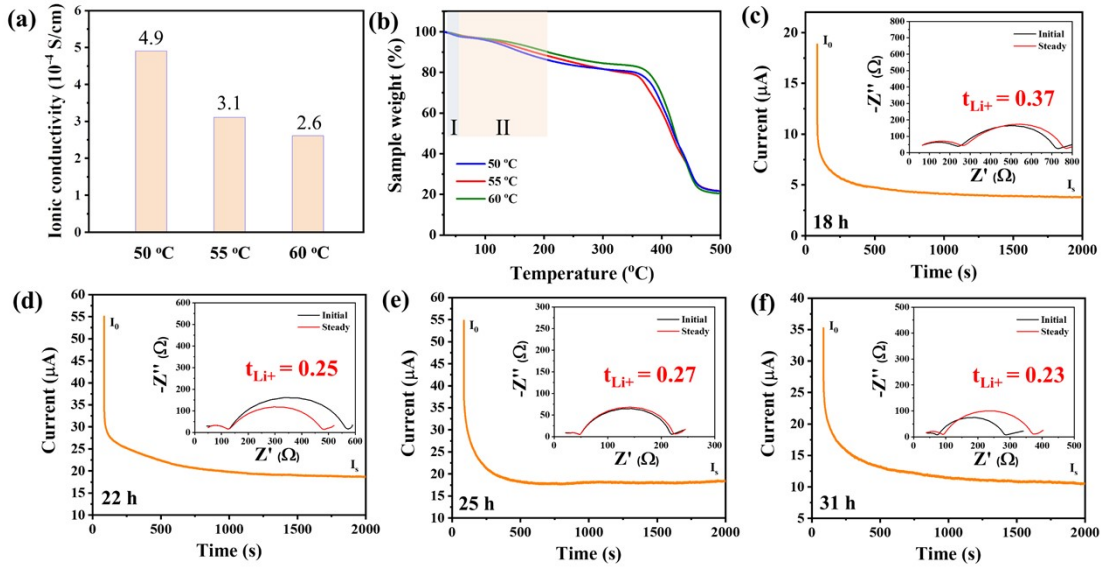

Fig. S3. (a) Ionic conductivities and (b) TGA result of P(VDF-TrFE-CTFE) SPEs prepared at varied temperatures. (c-f) Chronoamperometry profiles of Li/Li symmetrical cells using P(VDF-TrFE-CTFE) SPEs under a polarization voltage of 10 mV, and the EIS spectra before and after the polarization (see insets).

In addition, the SPEs films were prepared at different evaporation times ranging from 18 to 31 h under 55 °C. The transference number of lithium ion (t_{Li+}) was calculated from the results from Figs. S3c to S3f. The t_{Li+} is 0.37, 0.25, 0.27, and 0.23 when evaporation time is 18, 22, 25, and 31 h, respectively. When using a short evaporation time such as 18 and 22 h, the interfacial resistance of Li/P(VDF-TrFE-CTFE)/Li cell is around 500 to 700 Ω (insets of Fig. S3c and S3d), which is obviously higher than those using relatively long evaporation time such as 25 and 31 h (200 ~ 300 Ω, insets of Fig. S3e and S3f). The amount of residual DMF is higher using 18 and 22 h than that using 25 and 31 h (Fig. S11a), and severe side reactions between DMF in P(VDF-TrFE-CTFE) SPEs and Li metal would take place,[S3-S5]

which leads to a relatively higher interfacial resistance. Extending the evaporation time to 25 h, the amount of residual DMF would be decreased (Fig. S11a) and the continuous interfacial reaction between DMF and Li metal would be reduced. In consequence, the P(VDF-TrFE-CTFE) SPEs exhibits a greatly decreased interfacial resistance (inset of Fig. S3e). With the further decrease of the amount of residual DMF using evaporation time of 31 h, although the side reaction between P(VDF-TrFE-CTFE) and Li metal could be suppressed to a large extent, the solvation effects for the ion transport caused by residual DMF bound in P(VDF-TrFE-CTFE) SPEs is obviously reduced. As a result, the ionic conductivity and t_{Li+} for P(VDF-TrFE-CTFE) SPEs prepared under 31 h evaporation decrease compared to those of the SPEs prepared using 25 h (Figs. 2g, S3, and S11c). The above results mean that an appropriate amount of residual DMF is preferred for cell performance.

Therefore, this work employed the evaporation temperature of 55℃ and evaporation time of 25 h as processing conditions to prepare the P(VDF-TrFE-CTFE) SPEs for optimized battery performance.

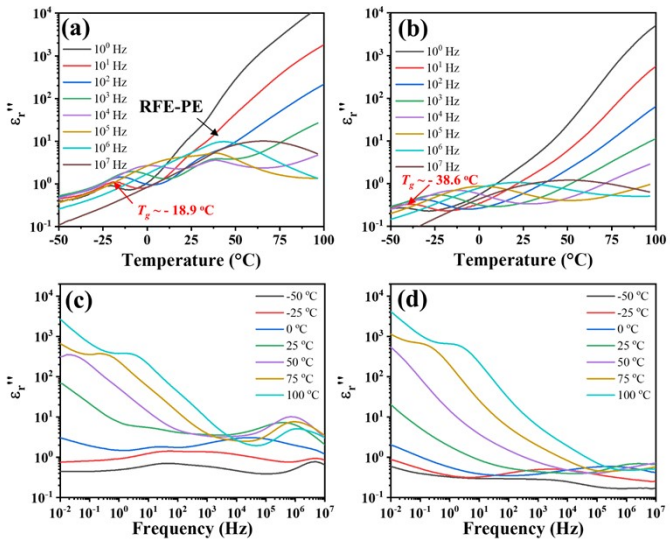

Fig. S4. Imaginary parts (ε_r'') of relative permittivity as a function of temperature at different frequencies for (a) P(VDF-TrFE-CTFE) and (b) PVDF. ε_r'' as a function of frequency at different temperatures for (c) P(VDF-TrFE-CTFE) and (d) PVDF.

Table S2. T_g of P(VDF-TrFE-CTFE) and PVDF obtained from Fig. S4 at different frequencies.

Frequency	10^0 Hz	10^1 Hz	10^2 Hz	10^3 Hz	10^4 Hz	10^5 Hz

$T_{g,\ P(VDF\text{-}TrFE\text{-}CTFE)}$	-20.9 °C	-18.9 °C	-15.2 °C	-8.7 °C	-3.1 °C	12.1 °C
$T_{g,\ PVDF}$	-50.0 °C	-38.6 °C	-31.2 °C	-23.7 °C	-14.4 °C	-1.9 °C

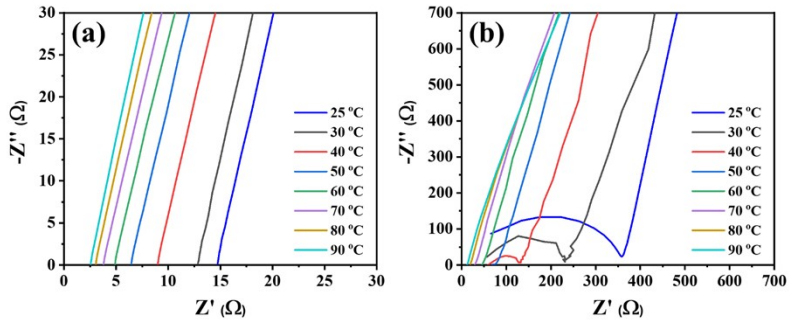

Fig. S5. EIS measurement of (a) P(VDF-TrFE-CTFE) and (b) PVDF electrolytes sandwiched by two stainless plates of steel (SS) at different temperatures.

Table S3. The electrochemical performance of Li metal batteries using different SPEs without any inorganic fillers.

Solid electrolyte	Ionic conductivity	Active material	Electrochemical performance	Ref
P(VDF-TrFE-CTFE)/LiTFSI	3.10×10^{-4} S/cm at 25 °C	$LiFePO_4$	146.0 mAh g^{-1} after 100 cycles under 0.5 C at 25 °C	**This work**
PVDF/LiTFSI	1.73×10^{-5} S/cm at 25 °C	$LiCoO_2$	20 mAh g^{-1} after 30 cycles under 0.05 mA cm^{-2} at 25 °C	S6
PVDF/LiFSI	1.18×10^{-4} S/cm at 25 °C	$LiCoO_2$	120 mAh g^{-1} after 100 cycles under 0.05 mA cm^{-2} at 25 °C	
P(VDF-HFP) /LiTFSI	1.4×10^{-5} S/cm at 20 °C	$LiFePO_4$	70 mAh g^{-1} after 100 cycles under 0.5 C at 25 °C	S7
P(VDF-HFP) /LiTFSI	$< 8.8 \times 10^{-5}$ S/cm at 25 °C	$LiFePO_4$	130 mAh g^{-1} after 100 cycles under 0.2 C at 55 °C	S8
P(VDF-HFP) /LiTFSI	1.23×10^{-6} S/cm at 25 °C	—	—	S9
P(VDF-HFP) /$LiClO_4$	7×10^{-5} S/cm at 25 °C	—	—	S10
P(VDF-HFP) /$LiClO_4$	1.4×10^{-5} S/cm at 25 °C	—	—	S11
PEO/LiTFSI	3.57×10^{-5} S/cm at 25 °C	$LiFePO_4$	130 mAh g^{-1} after 80 cycles under 0.1 C at 45 °C	S12
PEO/LiTFSI	5.4×10^{-5} S/cm at 30 °C	$LiFePO_4$	80 mAh g^{-1} after 100 cycles under 0.5 C at 60 °C	S13
PAN/$LiClO_4$	2.1×10^{-7} S/cm at 25 °C	—	—	S14

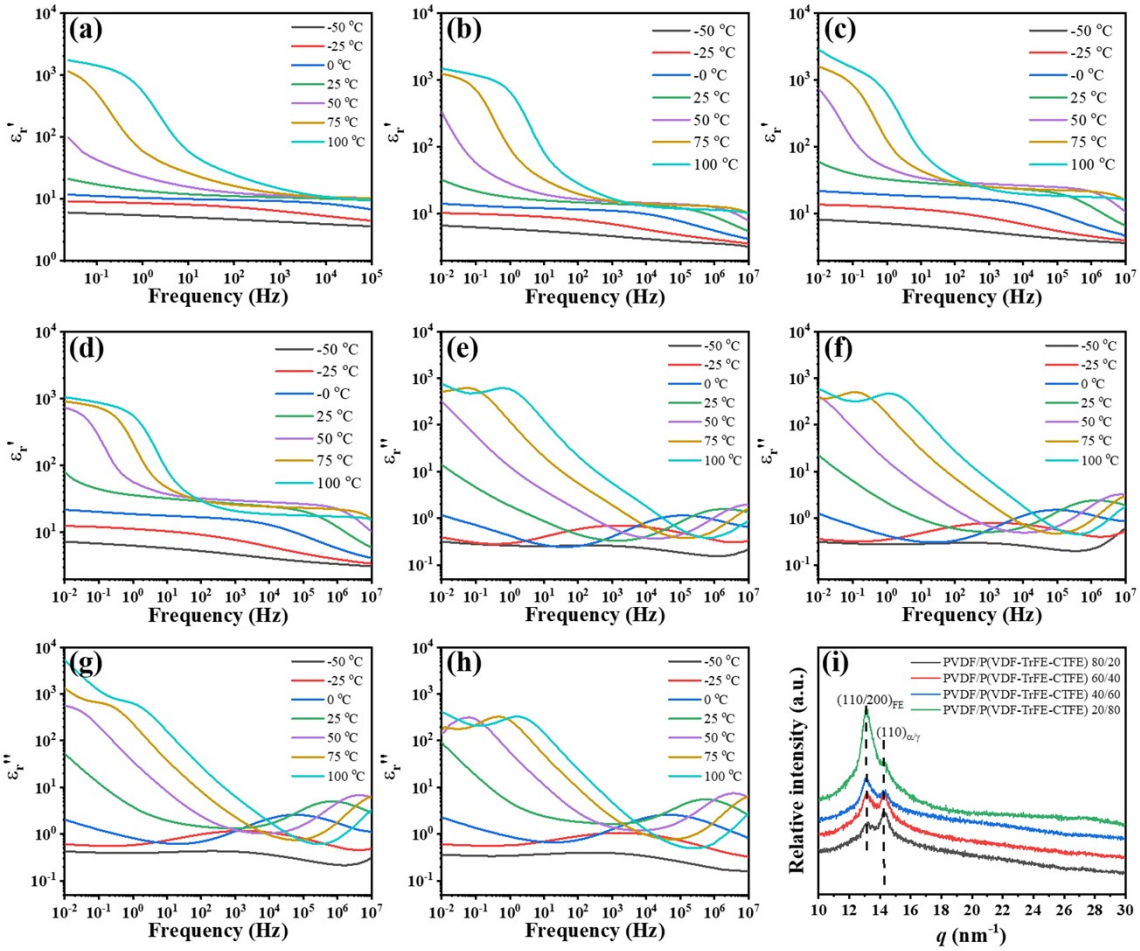

Fig. S6. ε_r' (a-d) and ε_r'' (e-h) as function of frequency at various temperatures for (a, e) PVDF/P(VDF-TrFE-CTFE) 20/80 wt%, (b, f) PVDF/P(VDF-TrFE-CTFE) 40/60 wt%, (c, g) PVDF/P(VDF-TrFE-CTFE) 60/40 wt%, and (d, h) PVDF/P(VDF-TrFE-CTFE) 80/20 wt% blends. (i) XRD curves of different PVDF/P(VDF-TrFE-CTFE) blends.

The XRD patterns of PVDF/P(VDF-TrFE-CTFE) blends are given in Fig. S6i. Two reflections at 13.1 and 14.2 nm^{-1} are observed, which correspond to the $(110/200)_{RFE}$ from P(VDF-TrFE-CTFE) and (110)α/γ from PVDF, respectively. The *d*-spacing of $(110/200)_{RFE}$ of PVDF/P(VDF-TrFE-CTFE) blends are calculated as 4.80 Å, which is comparable to that of P(VDF-TrFE-CTFE) (4.84 Å, Fig. 3f). This result indicates that the P(VDF-TrFE-CTFE) blends still show an RFE behavior, which increases the dielectric constant (Fig. 2h and 2i).

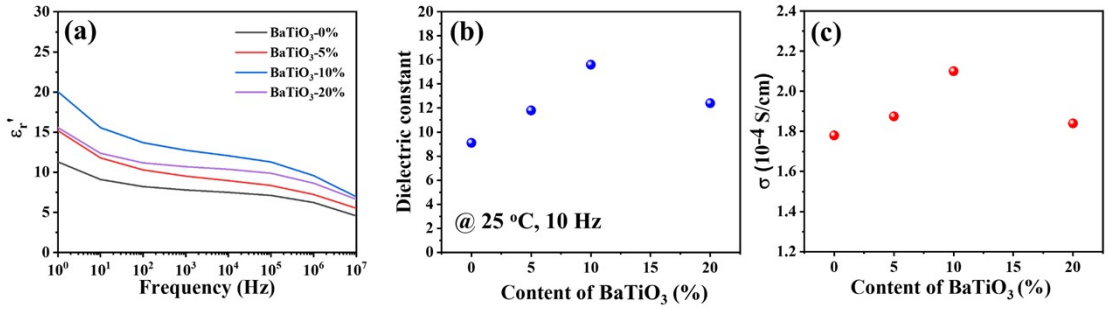

Fig. S7. (a) ε_r' as a function of frequency at 25 °C for PVDF/$BaTiO_3$ with different $BaTiO_3$ loadings. (b) Dielectric constants of PVDF/$BaTiO_3$ composites at different content of $BaTiO_3$ obtained from (a). (c) Ionic conductivities of PVDF/$BaTiO_3$-based electrolytes at different content of $BaTiO_3$.

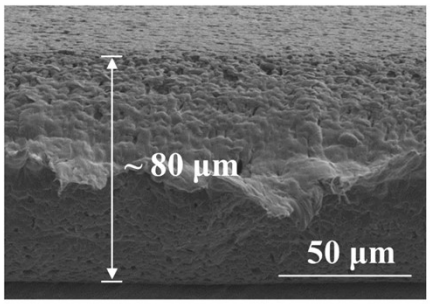

Fig. S8. SEM images of the cross-section of PVDF-based electrolytes.

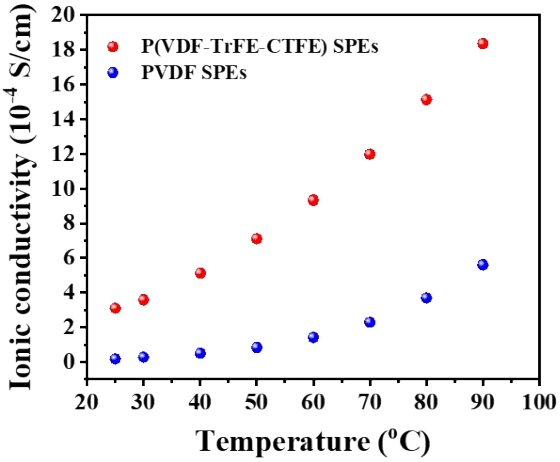

Fig. S9. Ionic conductivities of P(VDF-TrFE-CTFE) and PVDF SPEs at varied temperatures.

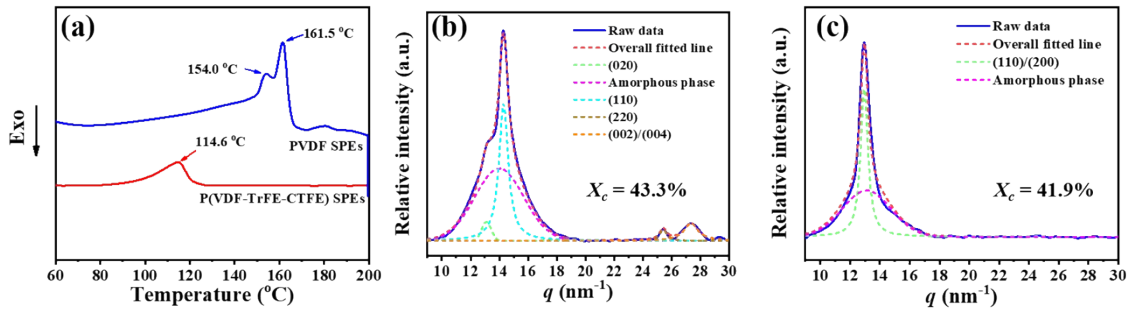

Fig. S10. (a) DSC 2nd heating curves of P(VDF-TrFE-CTFE) SPEs and PVDF SPEs. (b) Peak-fitting of XRD curves for (b) P(VDF-TrFE-CTFE) SPEs and (c) PVDF SPEs to calculate the crystallinity.

To Figure out the effect of residual DMF on the ionic conductivity, the P(VDF-TrFE-CTFE) and PVDF SPEs membranes with different amounts of residual DMF were prepared (**Fig. S11**a). It is easy to observe that the amount of residual DMF is always higher in PVDF electrolytes than that in P(VDF-TrFE-CTFE) electrolytes. As proved by the DFT calculation (Fig. 3j), this is because PVDF shows higher adsorption energy on DMF than P(VDF-TrFE-CTFE). In addition, no peak for free DMF is detected in the FTIR spectrum (Fig. S11b), suggesting the residual DMF is in bounded form and the prepared PVDF-based electrolytes are still in solid-state. We chose two samples with extremely low content of DMF residues (i.e. the ones prepared using 31 h evaporation, Fig. S11a) to measure the ionic conductivity and compared with the values reported in the Main article. The results show that the ionic conductivity of P(VDF-TrFE-CTFE) and PVDF SPEs decrease from 3.10×10^{-4} S cm^{-1} to 3.67×10^{-5} S cm^{-1}, and from 1.77×10^{-5} S cm^{-1} to 5.28×10^{-6} S cm^{-1}, respectively (Fig. 2 and S11c). It is worth noting that the P(VDF-TrFE-CTFE) SPEs with a lower amount of residual DMF still show a much higher ionic conductivity than PVDF SPEs, suggesting that the employment of P(VDF-TrFE-CTFE) with a high dielectric constant is a key factor for the greatly improved ionic conductivity for PVDF-based SPEs.

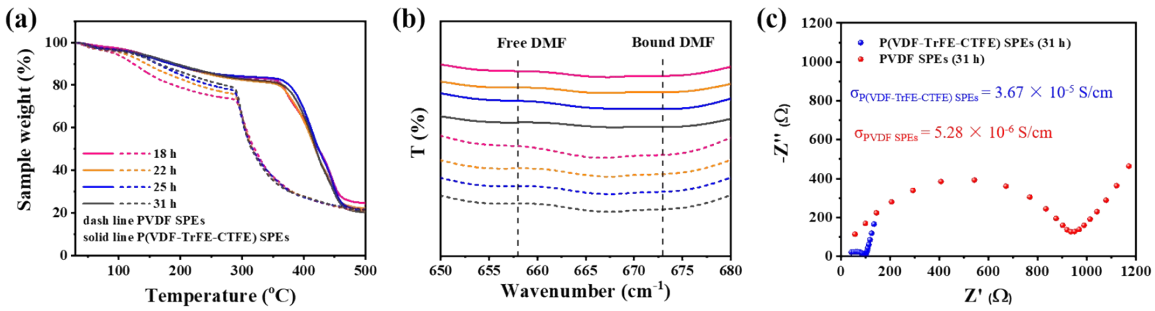

Fig. S11. (a) TGA of P(VDF-TrFE-CTFE) and PVDF SPEs prepared at 55 °C for different times. (b) FTIR spectra of DMF molecules in different P(VDF-TrFE-CTFE) and PVDF SPEs in (a). The FTIR peak positions for free DMF molecules are 658 cm^{-1}, which shifts to higher position at 673 cm^{-1}, indicating the residual DMF exists in a bounded form.[S11, S14] (c) EIS spectra of SS/SS cell based on P(VDF-TrFE-CTFE) and PVDF SPEs with solvent evaporation time of 31 h.

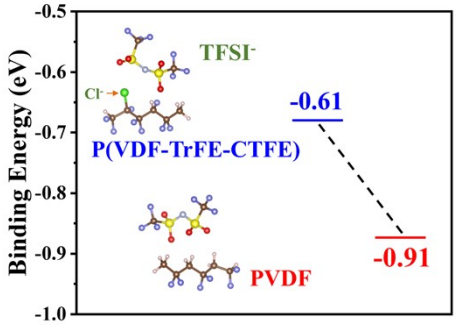

Fig. S12. The adsorption energy of $TFSI^-$ on P(VDF-TrFE-CTFE) and PVDF by DFT calculation.

The Raman spectra of PVDF/$BaTiO_3$ composites are provided in Fig. S13. From the peak-fitting results, the relative peak intensity of C_{coord} corresponding to the TFSI anions-coordinated Li^+ decreases with increasing of the $BaTiO_3$ filler from 0 wt% (Fig. 4e) to 10 wt% (Figs. S13a and S13b). That means more uncoordinated and free Li^+ are formed when the filler concentration climbs from 0 to 10 wt%. Further increasing the weight ratio of $BaTiO_3$ to 20 wt%, the relative peak intensity of C_{coord} decreases, probably because some $BaTiO_3$ are agglomerated. From Figs. 4e, S7, and S13, the composite electrolytes with higher dielectric constant show more free Li^+ and higher ionic conductivity. These results further confirm that the solid-state electrolyte with high dielectric constant promotes the dissociation of lithium salts.

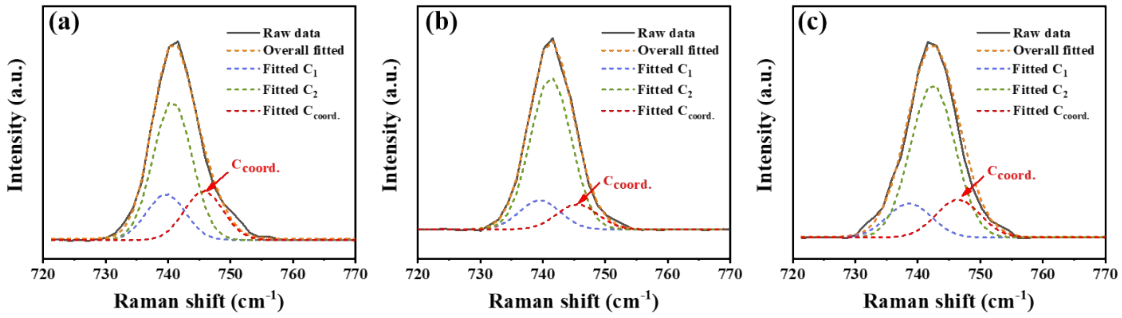

Fig. S13. Raman spectra of (a) PVDF/$BaTiO_3$-5 wt%, (b) PVDF/$BaTiO_3$-10 wt%, and (c) PVDF/$BaTiO_3$-20 wt% composite SPEs at 25 °C in the range of 720-770 cm^{-1}.

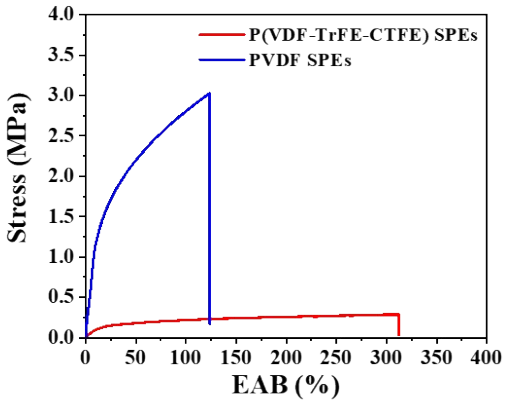

Fig. S14. Tensile properties of P(VDF-TrFE-CTFE) and PVDF SPEs. The stretching rate is 10 mm/min. The sample is 10 mm in width, 60 mm in length, and 0.1 mm in thickness.

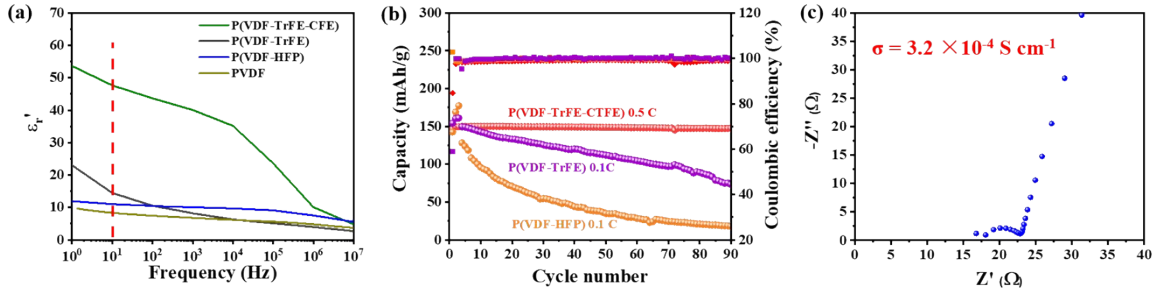

Fig. S15. (a) ε_r' as a function of frequency at 25 °C for different PVDF based co- and ter-polymers. (b) Cycling performance of $LiFePO_4$/Li batteries with P(VDF-TrFE-CTFE), P(VDF-TrFE), and P(VDF-HFP) SPEs at 25 °C. (c) EIS spectrum of SS/P(VDF-TrFE-CFE)/SS cell at 25 °C.

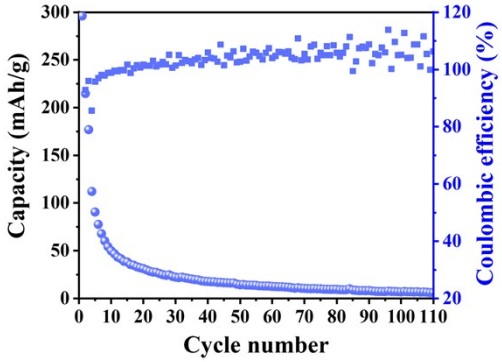

Fig. S16. Cycling performances for $LiFeO_4$/PVDF/Li battery at 0.1 C and 25 °C. The weight ratio of PVDF to LiTFSI is 3:5.

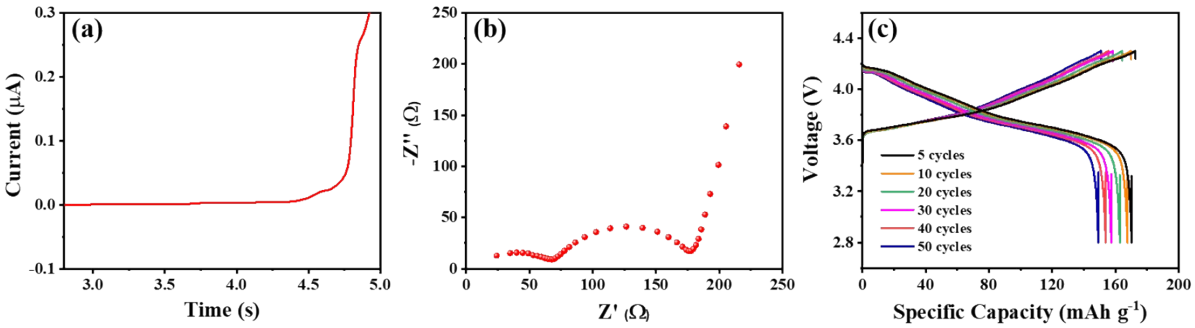

Fig. S17. (a) LSV curve of P(VDF-TrFE-CTFE) SPEs at 25 °C. (b) EIS spectra of the NCM811/P(VDF-TrFE-CTFE)/Li battery. (c) Charge-discharge voltage profiles of NCM811/P(VDF-TrFE-CTFE)/Li batteries at varied cycles. The batteries were performed at 0.1 C and 25 °C.

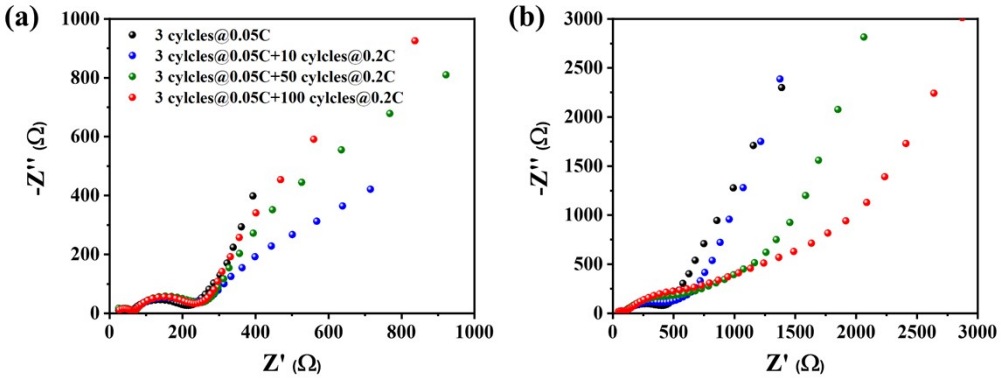

Fig. S18. The interfacial resistance of (a) $LiFeO_4$/P(VDF-TrFE-CTFE)/Li and (b) $LiFeO_4$/PVDF/Li cells at different cycles at 25 °C.

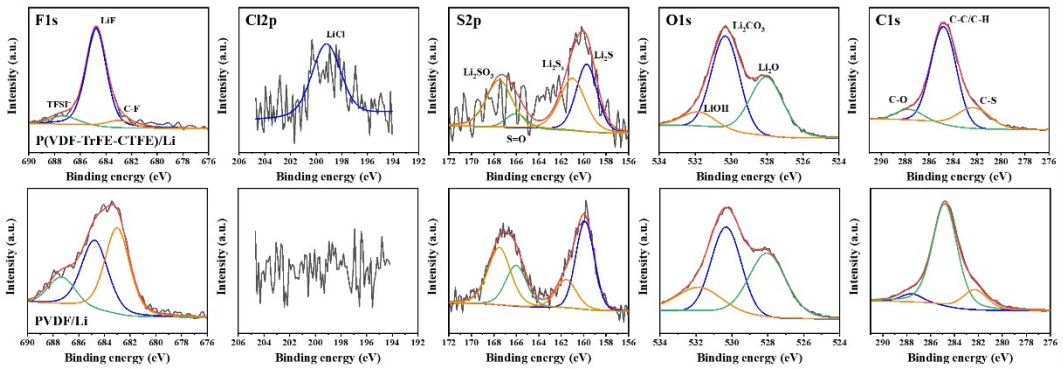

Fig. S19. F1s, Cl2p, S2p, O1s and C1s XPS spectra of Li anodes in LFP/PVDF/Li and LFP/P(VDF-TrFE-CTFE)/Li batteries after 100 cycles at 0.2 C and 25 °C.

For the LFP/P(VDF-TrFE-CTFE)/Li battery, the components of cycled Li surface mainly consist of LiF, Li_2CO_3, Li_2O, sulfur compounds, and LiCl, which are attributed to the interfacial reactions between $TFSI^-$ and Li metal, and the residue of P(VDF-TrFE-CTFE) on Li metal surface. Whereas, the LiCl peak is absent and LiF peak decreases greatly in the XPS of cycled Li surface from LFP/PVDF/Li battery compared to those from LFP/P(VDF-TrFE-CTFE)/Li battery. It was reported that the LiF could effectively prevent the dissociation of C-F bond from PVDF-based polymer and make the electrolytes stable during Li stripping-plating cycle.[6] The higher amount of LiF on the cycled Li anodes of LFP/P(VDF-TrFE-CTFE)/Li cell demonstrates the formation of a more stable interface between P(VDF-TrFE-CTFE) electrolytes and Li anodes, which contributes to a superior battery performance.

References

[S1] Yang, L. et al. Relaxor ferroelectric behavior from strong physical pinning in a poly (vinylidene fluoride-co-trifluoroethylene-co-chlorotrifluoroethylene) random terpolymer. *Macromolecules* **47**, 8119-8125 (2014).

[S2] Liu, W. Y. et al. Designing polymer-in-salt electrolyte and fully infiltrated 3d electrode for integrated solid-state lithium batteries. *Angew. Chem. Int. Ed.* **60**, 12931-12940 (2021).

[S3] Lang, J. L. et al. One-pot solution coating of high quality LiF layer to stabilize Li metal

anode. *Energy Storage Mater.* **16**, 85-90 (2019).

[S4] Bag, S. et al. LiF modified stable flexible PVDF-garnet hybrid electrolyte for high performance all-solid-state Li–S batteries. *Energy Storage Mater.* **24**, 198-207 (2020).

[S5] Zhang, X. et al. High cycling stability for solid-state li metal batteries via regulating solvation effect in poly(vinylidene fluoride)-based electrolytes. *Batter. Supercaps* **3**, 1-9 (2020).

[S6] Zhang, X. et al. Self-suppression of lithium dendrite in all-solid-state lithium metal batteries with poly (vinylidene difluoride)-based solid electrolytes. *Adv. Mater.* **31**, 1806082 (2019).

[S7] Li Y. et al. $Li_7La_3Zr_2O_{12}$ ceramic nanofiber-incorporated composite polymer electrolytes for lithium metal batteries. *J. Mater. Chem. A* **7**, 3391-3398 (2019).

[S8] Lu J. et al. Hybridizing poly (vinylidene fluoride-co-hexafluoropropylene) with $Li_{6.5}La_3Zr_{1.5}Ta_{0.5}O_{12}$ as a lithium-ion electrolyte for solid state lithium metal batteries. *Chem. Eng. J.* **367**, 230-238 (2019).

[S9] Zhang W. et al. A durable and safe solid-state lithium battery with a hybrid electrolyte membrane. *Nano Energy* **45**, 413-419 (2018).

[S10] Zhang X. et al. Synergistic coupling between $Li_{6.75}La_3Zr_{1.75}Ta_{0.25}O_{12}$ and poly (vinylidene fluoride) induces high ionic conductivity, mechanical strength, and thermal stability of solid composite electrolytes. *J. Am. Chem. Soc.* **139**, 13779-13785 (2017).

[S11] Sun Y. et al. Improving ionic conductivity with bimodal-sized $Li_7La_3Zr_2O_{12}$ fillers for composite polymer electrolytes. *ACS Appl. Mater. Interfaces* **11**, 12467-12475 (2019).

[S12] Wang, Z. P. et al. Low resistance-integrated all-solid-state battery achieved by

$Li_7La_3Zr_2O_{12}$ nanowire upgrading polyethylene oxide (PEO) composite electrolyte and PEO cathode binder. *Adv. Funct. Mater.* **29**, 1805301 (2018).

[S13] Wan J. et al. Ultrathin, flexible, solid polymer composite electrolyte enabled with aligned nanoporous host for lithium batteries. *Nat. Nanotechnol.* **14**, 705-711 (2019).

[S14] Liu, W. et al. Ionic conductivity enhancement of polymer electrolytes with ceramic nanowire fillers. *Nano Lett.* **15**, 2740-2745 (2015).